A&A 539, A75 (2012)
DOI: 10.1051/0004-6361/201117363

Astronomy & Astrophysics

The inner heliosheath source for keV-ENAs observed with IBEX

Shock-processed downstream pick-up ions

M. Siewert[1], H.-J. Fahr[1], D. J. McComas[2], and N. A. Schwadron[3]

[1] Argelander Institut für Astronomie der Universität Bonn, Abteilung f. Astrophysik und Extraterrestrische Forschung, Auf dem Huegel 71, 53121 Bonn, Germany
e-mail: msiewert@astro.uni-bonn.de
[2] Southwest Research Institute, San Antonio, TX; and University of Texas, San Antonio, San Antonio, TX, USA
[3] Department of Astronomy, University of New Hampshire, Durham, NH, USA

Received 28 May 2011 / Accepted 16 December 2011

ABSTRACT

Context. The "IBEX ribbon" feature provides significant challenges to theoretical modeling attempts of the outer heliosphere. Classical ENA production by shock-processed nonthermal tails results in no relevant ENA signatures, mainly due to the downstream solar wind proton temperature observed by the Voyagers being one order of magnitude smaller than expected from the classical monofluid shock model.

Aims. Here, we therefore study shock-processed pick-up ions (PUIs) in the inner heliosheath resulting from a multifluid shock model as a source of keV-energetic ENAs as have been detected by the IBEX mission. Unlike previous studies, we apply a semikinetic multifluid shock model, which did prove useful in explaining the apparent temperature discrepancy in the past.

Methods. To convert upstream into downstream pick-up ions, we use both kinetic and multifluid theories describing the solar wind termination shock (TS) transition. This allows us to obtain the downstream PUI distribution function as a function of classical shock properties, such as the local magnetic field tilt angle and the compression ratio. In addition, this kinetic model also allows to derive a formulation of latitude- and longitude-dependent spectral intensities between 1 and 100 keV, a region which is not covered by missions such as the Voyagers and needs to be covered by theoretical considerations.

Results. After converting shock-processed PUIs to ENAs by charge exchange with cold H-atoms, we find keV ENA fluxes of the same order of magnitude as those observed by IBEX. These fluxes also exhibit a pronounced ring-type feature, with about the correct ratio of ring-to-nose intensities, producing encouraging overall agreement with IBEX data, potential of further improvement.

Key words. magnetohydrodynamics (MHD) – shock waves – plasmas – solar wind

1. Introduction

Launched in late 2008, the Interstellar Boundary EXplorer (IBEX) is designed to detect energetic neutral atoms generated inside, near and beyond the heliospheric boundary layer, i.e. the heliopause (McComas et al. 2004, 2006, 2009b). Observing the entire sky in only six months, the mission is not restricted to the detection of energy-resolved fluxes of neutral atoms from different directions, but it may, by temporal resolution, also enable studies of the dynamic behaviour of the heliosphere on timescales greater than half a year (McComas et al. 2010, and even smaller timescales towards the poles; see Reisenfeld et al. 2009), offering an enhanced resolution of solar cycle-induced effects.

The first half-year results were published in late 2009 (McComas et al. 2009a; Schwadron et al. 2009; Funsten et al. 2009; Fuselier et al. 2009), which clearly proved the presence of a completely unexpected phenomenon, a distinct ENA emissive feature at the sky, which has become known as the "IBEX ribbon". This ribbon, which consists of a special discrete region in the sky observed in essentially all energy bands measured by the IBEX ENA detectors, was completely absent in all model predictions before 2009 (Gruntman et al. 2001; Scherer & Fahr 2003; Fahr & Scherer 2004; Heerikhuisen et al. 2008; Sternal et al. 2008; Prested et al. 2008; Izmodenov et al. 2009; Lee et al. 2009). New ideas and models aiming to explain this feature have started to emerge since then (see e.g. McComas et al. 2009a; Schwadron et al. 2009; McComas et al. 2010; Heerikhuisen et al. 2010; Grzedzielski et al. 2010; Chalov et al. 2010); however, several properties of the data have proven especially challenging. First, the ribbon intensity seems most pronounced at ∼1 keV, while the shape of feature seems to broaden at higher energies, and second, when fitting the ENA flux data with power laws, the ribbon does not appear as a special feature in the resulting power law index distribution (McComas et al. 2009a). One straightforward way to explain these two properties would be to assume that the physical processes generating the ribbon – besides of their absolute rates – are qualitatively and physically similar to those operating in the remaining regions of the sky, thus resulting in the same qualitative spectral shape, and that the only difference between both regions might be the spectral intensity of ENA sources.

Deriving an improved ENA flux model taking into account these properties of the data is one of the most ambitious research topics in heliospheric astrophysics today (McComas et al. 2010). Possible explanations which are currently under investigation range from unusual magnetic field behaviours in the local interstellar medium (LISM) (Heerikhuisen et al. 2010; Chalov et al. 2010) or properties of the interstellar interface (Grzedzielski et al. 2010), modified thermal pressures (McComas et al. 2009a; Funsten et al. 2009; Krimigis et al. 2009) to a delicate

combination of processes in the local medium, e.g. due to pitch angle anisotropic pick-up ions in the outer heliosphere or the outer heliosheath. Pitch-angle anisotropic ions introduce an additional parameter to the system of Rankine-Hugoniot jump conditions (a second pressure, or, equivalently, a second temperature), resulting in an underdetermined system of equations, requiring additional modeling input (see e.g. Erkaev et al. 2000; Vogl et al. 2003; Siewert & Fahr 2008). However, without special ad hoc assumptions concerning the responsible kappa-character of the ion distribution functions, or vanishing pitch-angle scattering, none of these explanations is able to represent sufficiently high spectral ENA-flux intensities at keV energies.

In this study, we focus on a model where the ENAs are generated on the near downstream side of the solar wind termination shock, where local behaviour such as the strength and orientation of the frozen-in shocked solar wind magnetic field leads to a strong modification of the local downstream plasma properties, such as the particle number density, the ion distribution function and especially the temperature of the plasma downstream of the termination shock. A sufficiently hot plasma will then be able to generate ENAs at energies larger than 1 keV originating from the supra-thermal flanks, with the temperature itself determining the number of energetic protons serving as seeds for keV-ENAs. This study is similar to earlier work by Prested et al. (2010), who also studied ENAs generated in the inner heliosheath. The main differences between their results and the present study originate from differences in several areas mostly related to the relevance of transition phenomena at the termination shock (TS). We introduce these details of our model identifying those physical parameters which are relevant for the ENA production process in the following section.

2. Energetic pickup ions

In this paper, we study ENAs generated in resonant charge exchange processes,

$$p^* + n \rightarrow n^* + p, \tag{1}$$

where the asterisk denotes an energetic particle ($E = \frac{1}{2}mv^2 \simeq 1$ keV). In this process, only an (essentially massless) electron is exchanged, and therefore, the resulting ENAs possess the same energies as the seed protons. In the relevant energy region, contributions from the thermal solar wind are negligibly small, and the major energetic protons are found in the Pick-Up Ion (PUI) component.

One specific complication which appears in all approaches to PUI-like particles faster than the solar wind speed is that no observational data exists in the region between 10 and 100 keV. Conventional PUIs are injected at the solar wind speed and cooling from there, not contributing to the energy region of interest to this study. When going to higher energies, the next relevant process is the injection of ACRs at the solar wind termination shock, which however occurs at energies of o(1 MeV). This energy region is covered by the Voyager instruments to energies as low as o(40−100 keV), leaving a clear gap in both observations and source processes, which should be dominated exclusively by kinetic (i.e. theoretical) models describing the cooling processes acting on ACRs.

In the paper by Fahr et al. (2009), the authors studied one specific model for the description of this gap, based on the concept that shock-generated Anomalous Cosmic Ray particles (ACRs) diffuse inwards from the shock while being modulated in energy due to adiabatic cooling processes. These authors showed that with the loss of particle energy and the associated decrease of the spatial diffusion coefficient, these ACRs lose their diffusive mobility and are finally again co-convected with the solar wind like pick-up ions. Within the framework of conventional ACR modulation theory, this process, obvious from the divergence of the ACR streaming, leads to local sinks in the ACR population. Adopting 10^2 keV as the critical energy to bind the lowest energy population of ACR ions to the highest energy population of pick-up ions allows us to consider this sink in the ACR population as a source for the pick-up ion population. With this additional ACR-induced pick-up ion injection term, and without need of any energy-diffusion process, the resulting pick-up ion distribution function was derived in an analytic form by solving the Boltzmann-Vlasow transport equation for this scenario.

According to the model used by Fahr et al. (2009), an analytical solution of the ACR transport equation, when enhanced by an apropriate ACR-induced source term, is given by

$$f_{\rm pui}(v,r) = \frac{\Lambda}{2\pi} n_{\rm p,E} U^2 \left(\frac{r_{\rm E}}{r}\right) v^{-5} H(U-v) + \frac{1}{9\pi} p_{\rm pui}^3 f_{\rm const}^{\rm ACR} v_{\rm pui} v^{-4}, \tag{2}$$

with $1 \times 10^{-3} \leq \Lambda = \sigma_{\rm ex} n_{H,\infty} r_{\rm E} \leq 3 \times 10^{-3}$ being a constant determined by the interstellar H-atom density $n_{\rm H,\infty}$, where $n_{\rm p,E}$ is the solar wind proton density at $r = r_{\rm E} = 1$ AU, U is the solar wind bulk velocity, and $p_{\rm pui}$, respectively $v_{\rm pui}$, are the critical momentum and velocity of ions injected from the ACR regime. The quantity $f_{\rm const}^{\rm ACR}$ is the constant value of the ACR distribution function at $p = p_{\rm pui}$.

The second term (proportional to v^{-4}), which follows from PUIs cooling downwards from the Anomalous Cosmic Ray (ACR) regime, has already been studied (Fahr et al. 2011), resulting in an ENA emission feature pronounced in the flanks of the heliospheric shock and more heliotailward (while the IBEX ribbon is found closer to the nose). In this study, we focus on the first term in Eq. (2), i.e. the regular PUI component which is then convected across the TS. As we demonstrate in more detail later in this paper, there are several elementary effects which follow from the basic microphysics of the shock transition which modulate the regular PUI component in a way favoring keV-ENA production.

Prested et al. (2010) selected a different approach to this distribution function, applying κ-distributions which are observationally suggested by Voyager-1/-2 Decker et al. (2005, 2008); Richardson et al. (2008), with a velocity distribution power index of $\kappa \simeq -5$. They assumed that suprathermal tail ions are then convected across the TS, taking the thermal solar wind proton component and convecting them across the shock, while assuming that the κ-index of the suprathermal tail remains constant. While this approach is acceptable in the sense that suprathermal tails are used to describe the energy region above 1 keV, they may mis-represent some of the microphysical properties of the solar wind termination shock.

One specific property which requires more careful studies is the temperature of downstream solar wind protons, which have been found to be colder by one order of magnitude than expected from monofluid MHD theory (see e.g. Richardson et al. 2008) for the initial discovery; for a theoretical treatment of this problem, see e.g. Fahr & Chalov (2008). In order to generate keV ENAs, the observed solar wind proton temperature of 10^5 K is too small by one order of magnitude. Therefore, generating a significant amount of 1 keV "parent" ions require a description where pick-up ions are converted separately (i.e. not via

a kappa-tail) into suprathermal keV energetic ions downstream of the TS. In addition, solar wind protons still appear supersonic downstream, which needs to be explained by any theoretical model as well. One way to resolve both of these problems at the same time is the multifluid description by Fahr & Chalov (2008), which shows that due to the conservation of the ion magnetic moment at the shock passage, the pick-up ions definitely gain much more energy than the cool solar wind protons. If this is taken into account, the downstream ions cannot be represented by kappa-distributed RH-shocked solar wind protons, but by heated pick-up ions with a downstream pressure given by

$$P_{\mathrm{pui},2} = s\frac{2s+1}{3}P_{\mathrm{pui},1}, \tag{3}$$

where s is the compression ratio and $P_{\mathrm{pui},1}$ is the upstream PUI pressure. Without this multi-fluid approach, it is not possible to obtain 10^6 K downstream solar wind protons as expected from the standard monofluid Rankine-Hugoniot model.

This conversion of upstream into downstream PUIs in fact needs a consistent multifluid treatment of the shock from which we first obtain the PUI downstream pressure. To convert this pressure into spectral PUI fluxes, we need to assume a distinct form of a distribution function which, in view of VOY-2 results by Decker et al. (2008), which we adopt as power laws. Power laws were also obtained from the solution of the PUI transport equation obtained by Fahr et al. (2009, see Eq. (2)), which was found to allow an extension of the energetic proton distribution function to ion velocities much higher than the solar wind speed. The PUI part of the distribution function is, of course, observationally accessible, and does not require an additional theoretical treatment. However, the most important aspect of our approach is the theoretical description of the downstream PUI pressure that depends on the magnetic field configuration at the termination shock, i.e. the tilt angle of the upstream field with respect to the shock normal. The underlying formalism does not explicitly depend on the spectral shape, and therefore, the power law used by us could easily be replaced by a different distribution function, e.g. a secondary, hot Maxwellian. The spectral shape must be expected to reflect in the spectral form of the resulting ENA fluxes, but the present study only evaluates ENA fluxes at o(1 keV), where the highest ENA fluxes have been observed by IBEX-High.

The conservation of the magnetic moment, which provides the foundations of the multifluid shock model, was first used by a semikinetic model developed by Siewert & Fahr (2008), where it was found that the individual ion velocities are scaled by a constant factor that only depends on the general parameters of the shock; this means that energetic upstream ions (which make up the nonthermal tail) will gain proportionally more thermal energy than low-energetic (thermal) upstream ions.

2.1. An analytical description of downstream processed PUIs

In the current study, we focus on "classical" PUIs, i.e. the first term in Eq. (2). Since upstream PUIs are marginally subsonic, i.e. $M_{\mathrm{pui},1} = \sqrt{\rho_{\mathrm{pui},1}U_1^2/(\gamma P_{\mathrm{pui},1})} \simeq 1$ (see Fahr & Chalov 2008; Lee et al. 2009), they, radially co-convected with the supersonic solar wind, and are essentially unable to produce appropriate ENAs (via charge transfer with cold interstellar H-atoms) that can move back towards the sun, while at the same time keeping energies of the order of 1 KeV or more in the solar rest frame. This frame-of-reference effect can be explained by noting that the distribution function (Eq. (2)) is defined in a reference frame co-moving outwards with the solar wind plasma, with a relative velocity U along the line of sight between the observer and the plasma. Ions with a velocity of $v = \sqrt{2E/m_{\mathrm{p}}}$ in this rest frame convect outwards with the solar wind and arrive in the observer's rest frame (at earth, i.e. roughly the sun) with a velocity of

$$v_{\mathrm{obs}} = v_{\mathrm{ena}} - U = U\left(\frac{v_{\mathrm{ena}}}{U} - 1\right). \tag{4}$$

Due to this frame-of-reference effect, it follows from the first term in Eq. (2) that there is no significant contribution to the observed ENA fluxes from the upstream side of the TS, since the distribution function is cut off at U (i.e. in the observers rest frame, the fastest particles available due to this term are at rest). For this reason, we do not need to take these upstream ions into account as relevant IBEX ENA sources here, and focus this study on downstream PUIs instead. After passing throughh the termination shock, these PUIs gain enough thermal energy from the conversion of kinetic energy of the supersonic wind so that downstream of the shock, the shock-induced suprathermal distribution function is able to produce ENAs propagating back towards the sun with energies of $E = o$(1 keV).

In order to quantitatively describe PUIs in the region downstream of the termination shock, one has to draw information both from (magneto-)hydrodynamic fluid concepts and from kinetic studies taking into account the transformation of individual ion velocities at the shock passage. As a first step towards this required information, Fahr & Chalov (2008) found that, within a consistent two-fluid hydrodynamic solar wind model (i.e. solar wind ions and PUIs coupled to each other), the resulting compression ratio of the termination shocks (see their Fig. 2) is related to the upstream PUI Mach number $M_{\mathrm{pui},1}$ through the relation

$$s(M_{\mathrm{pui},1}) = 2.6\sqrt{M_{\mathrm{pui},1}}. \tag{5}$$

In addition, Fahr & Siewert (2010b) showed that, using kinetic studies and the assumption of conserved ion invariants at the shock passage, the PUI pressure downstream of the shock after reisotropisation of the initially pitch-angle anisotropic downstream ion distribution is given by

$$P_{\mathrm{pui},2} = s\left[\frac{2}{3}\sqrt{\cos^2\theta + s^2\sin^2\theta} + \frac{1}{3}\frac{s^2}{\cos^2\theta + s^2\sin^2\theta}\right]P_{\mathrm{pui},1}, \tag{6}$$

where s is the shock compression ratio and $\theta = \angle(\boldsymbol{B}, \boldsymbol{n})$ is the tilt angle between the shock normal vector and the local upstream magnetic field. This expression can be simplified by introducing

$$G(s,\theta) = \cos^2\theta + s^2\sin^2\theta \tag{7}$$

and

$$C(s,\theta) = \frac{2}{3}\sqrt{G(s,\theta)} + \frac{1}{3}\frac{s^2}{G(s,\theta)}, \tag{8}$$

to obtain the more compact equation

$$P_{\mathrm{pui},2} = sC(s,\theta)P_{\mathrm{pui},1}. \tag{9}$$

According to observations made by many different spaceprobes, providing an almost uninterrupted observation (see e.g. Gloeckler 2003; Fisk & Gloeckler 2008; Dayeh et al. 2009), PUIs both upstream and downstream appear to have a power law

distribution function with a power index averaging (−5), thus given by

$$f_{\rm pui}(v) = f_{\rm pui,0}\left(\frac{v}{v_0}\right)^{-5}, \tag{10}$$

where the normalization factor is given by

$$f_{\rm pui,0} = \frac{n_{\rm pui}}{2\pi v_0^3}. \tag{11}$$

Strictly speaking, these observations do not cover the entire energy range down to PUI energies (o(1 keV)), but only to 40 keV, leaving more than one order of magnitude which is not covered by observations. However, the general power index of −5 is, essentially, the same as the power index derived in the kinetic model by Fahr et al. (2009), and therefore, it is reasonable to assume that the power law continues downward to PUI injection energies. Nevertheless, is must be kept in mind that this region is not covered by independent experimental data; in fact, IBEX (and, to some extent, Cassini) might be the first missions to trace this energy region (see e.g. Schwadron et al. 2011). Studying the spectral behaviour of this process will be the goal of a separate publication.

After this intermission, we continue deriving the analytical form of the distribution function. Continuing from our previous results, we obtain the following simple expressions for the PUI density and pressure (which are defined as moments of this power law distribution function, see e.g. Fahr 2007)

$$n_{\rm pui} = 2\pi f_{\rm pui,0} v_0^3 \tag{12}$$

and

$$P_{\rm pui} = 4\pi f_{\rm pui,0}\frac{m}{2}v_0^5 \ln\left(\frac{v_\infty}{v_0}\right) = n_{\rm pui} m v_0^2 \ln\left(\frac{v_\infty}{v_0}\right), \tag{13}$$

where v_∞ and v_0 are upper and lower physical cutoff values of the particle velocity distribution $f_{\rm pui}(v)$. Using Eqs. (12) and (13) then results in

$$n_{\rm pui} = \frac{P_{\rm pui}}{m v_0^2 \ln(v_\infty/v_0)}. \tag{14}$$

Assuming that Eq. (11) defines the normalising factor on the upstream side ($f_{\rm pui,0,1}$), we now derive the downstream normalization factor as a function of upstream parameters. Using Eqs. (14) and (9), it follows that

$$n_{\rm pui,2} = \frac{sC(s,\theta)P_{\rm pui,1}}{m v_{0,2}^2 \ln\left(\frac{v_{\infty,2}}{v_{0,2}}\right)}, \tag{15}$$

and thus the normalization factor turns out as

$$f_{\rm pui,0,2} = \frac{sC(s,\theta)P_{\rm pui,1}}{2\pi m v_{0,2}^5 \ln\left(\frac{v_{\infty,2}}{v_{0,2}}\right)}. \tag{16}$$

This expression may be simplified further by applying Eq. (13), resulting in

$$f_{\rm pui,0,2} = \frac{sC(s,\theta)n_{\rm pui,1}v_{0,1}^2 \ln\left(\frac{v_{\infty,1}}{v_{0,1}}\right)}{2\pi v_{0,2}^5 \ln\left(\frac{v_{\infty,2}}{v_{0,2}}\right)}. \tag{17}$$

Next, we apply another kinetic relation derived by Fahr & Siewert (2010b) for the transformation of upstream into downstream velocities,

$$v_2^2 = v_1^2 C(s,\theta), \tag{18}$$

and the downstream normalization simplifies to

$$f_{\rm pui,0,2} = \frac{sn_{\rm pui,1}}{2\pi C^{3/2}(s,\theta)v_{0,1}^3}, \tag{19}$$

where the logarithms cancel out due to $v_{\infty,1}/v_{0,1} = v_{\infty,2}/v_{0,2}$. Therefore, the only power-law cutoff parameter influencing the system is the lower velocity border $v_{0,1}$. Adapting the value $v_{0,1} = U_1$ on the upstream side (which corresponds to the velocity difference between the solar wind frame and the observers frame), we obtain

$$f_{\rm pui,0,2} = \frac{sn_{\rm pui}}{2\pi U_1^3}C^{-3/2}(s,\theta) = sf_{\rm pui,0,1}C^{-3/2}(s,\theta), \tag{20}$$

and the full downstream pick-up ion distribution function is given by

$$\begin{aligned} f_{\rm pui,2}(v_2) &= \frac{sn_{\rm pui}}{2\pi U_1^3}C^{-3/2}(s,\theta)\left(\frac{v_1}{U_1}\right)^{-5} \\ &= sC^{-3/2}(s,\theta)f_{\rm pui,0,1}\left(\frac{v_1}{U_1}\right)^{-5}. \end{aligned} \tag{21}$$

i.e. the main difference between the upstream and downstream distribution functions – besides the transformation of the individual particle velocities – is a factor of

$$sC^{-3/2}(s,\theta). \tag{22}$$

This result is consistent with the results obtained by Fahr & Siewert (2010a), who found that

$$f_2(v_2) = sC^{-3/2}(s,\theta)f_1\left(\frac{v_2}{\sqrt{C(s,\theta)}}\right), \tag{23}$$

i.e. we obtain the same renormaliation factor. Great care must be taken, however, when transforming the parameter $U_1 = v_{0,1}$ in this relation, which transforms as an individual particle velocity (i.e. with $\sqrt{C}$), and not with the basic compression ratio (i.e. s^{-1}). Therefore, we additionally obtain $v_2/v_{0,2} = v_1/v_{0,1}$ and

$$f_2\left(\frac{v_2}{v_{0,2}}\right) = sC^{-3/2}(s,\theta)f_1\left(\frac{v_1}{v_{0,1}}\right). \tag{24}$$

In other words, we do not need to transform upstream velocities into downstream ones, but we can keep working exclusively with upstream velocities and $v_{0,1} = U_1$, and the only downstream parameter appearing in this expression is the MHD compression ratio s. For this reason, we omit the subscripts 1 and 2 at individual particle velocities from this point on.

Next, we introduce the pick-up ion abundance by $\xi = n_{\rm pui}/n_{\rm p}$ which, as derived by Fahr & Ruciński (1999), is independent on the solar wind velocity U,

$$\xi(r,\beta) = 1 - \exp\left[-\int_{r_0}^{r}\sigma_{\rm ex}n_{\rm H}(r',\beta){\rm d}r'\right], \tag{25}$$

where β is the angle between the radian vector and the upwind direction with the relation $\cos\beta = \cos\delta\cos\alpha$, the upwind direction given by $\{\alpha = 0; \delta = 0\}$. The angle α is the right ascension (i.e. (α,δ) denotes the ecliptic coordinate system). This allows transformation of Eq. (21) into the form

$$f_{\rm pui,2}(v) = \frac{s\xi_{\rm s}(\alpha,\delta)n_{\rm p,E}}{2\pi U_1^3 C^{3/2}(s,\theta)}\left(\frac{r_{\rm E}}{r_{\rm s}(\alpha,\delta)}\right)^2\left(\frac{v}{U_1}\right)^{-5} \tag{26}$$

where we have introduced the ratio of the solar distances of the earth and the termination shock, i.e. r_E/r_s, to account for the different solar wind proton densities at different locations of the TS (see e.g. McComas & Schwadron 2006). The subscript s at $r_s(\alpha,\delta)$ denotes the *s*hock distance in the direction $\{\alpha,\delta\}$ (see Sect. 3.4.1) for the models applied by us). Keeping in mind that the PUI abundance at the shock position essentially turns out to be independent of the direction, given by $\xi(\alpha,\delta) \simeq \xi_s(0,0) \simeq 0.15$ (see Fahr & Ruciński 1999; Fahr et al. 2011), we finally obtain the above expression in the following form

$$f_{\mathrm{pui},2}(v) = \frac{s\xi_s(0,0)n_{\mathrm{p,E}}}{2\pi U_1^3 C^{3/2}(s,\theta)}\left(\frac{r_E}{r_s(\alpha,\delta)}\right)^2\left(\frac{v}{U_1}\right)^{-5}. \tag{27}$$

Comparing this result with Eq. (21), we see that the new parameterisation (depending on n_p instead of n_{pui}) may be absorbed in the normalization factor

$$f_{\mathrm{pui},0,1} = \frac{\xi_s(0,0)n_{\mathrm{p,E}}}{2\pi U_1^3}\left(\frac{r_E}{r_s(\alpha,\delta)}\right)^2 = \frac{\xi_s(0,0)n_{\mathrm{p,E}}(r_s)}{2\pi U_1^3}. \tag{28}$$

This expression is a function of the quantity $r_s(\alpha,\delta)$ (which may be derived from a heliospheric model) and the two shock parameters $s = \rho_2/\rho_1$ and $\theta = \angle(\boldsymbol{n},\boldsymbol{B})$, which additionally require models for the solar wind termination shock. It is important to remember that the compression ratio s is a function of the upstream PUI Mach number given by Eq. (5), eliminating the requirement to solve the jump conditions at the TS, and allowing us to describe the PUIs on the downstream side of the shock exclusively as a function of upstream parameters. In other, more realistic solar wind models, especially those based on magnetohydrodynamic concepts and/or more fluid components, this final point may be more complicated, i.e. solving the specific jump conditions might nevertheless be necessary, though.

3. The integrated ENA flux in the observers rest frame

3.1. The inner heliosphere

In this section, we derive the ENA fluxes produced by resonant charge exchange with the PUI ion distributions discussed above, transforming an energetic ion into an ENA with essentially the same velocity vector. Making the additional assumption (which is in fact very well supported by estimates made by Fahr & Scherer 2004) that ENAs generated will not be reionised during their passage over $o(100\ \mathrm{AU})$ from the TS to the earthbound observer, we define these fluxes with a line-of-sight integral

$$\begin{aligned}\Phi_{\mathrm{ENA}}(v_{\mathrm{obs}},\alpha,\delta) &= \int_{r_0}^{r_1}\frac{\mathrm{d}r}{v_{\mathrm{ENA}}}P_{\mathrm{ENA}}v_{\mathrm{ENA}}\\ &= \int_{r_0}^{r_1}\mathrm{d}r\, j_1(E_{4.5})\sigma_{\mathrm{ex}}(E_{4.5})n_{\mathrm{H}}.\end{aligned} \tag{29}$$

Here we have introduced the differential energy flux $j(E)$ as defined by e.g. Lee et al. (2009)

$$j(E) = \frac{2}{m_p^2}Ef(E) = \frac{1}{m_p}v^2 f(v) \tag{30}$$

with $f(E)$ being the ion energy distribution function normalized to $n = 4\pi\int f(E)\sqrt{E}\mathrm{d}E$.

Due to the frame-of-reference effect discussed above the upstream ions will not contribute to the observed ENA fluxes at keV-energies. The downstream contribution, on the other hand, is enhanced (with respect to a comparable upstream contribution) due to a higher particle number density and temperature, i.e. the total ENA flux is well approximated by

$$\begin{aligned}\Phi_{\mathrm{ENA,tot}}(v_{\mathrm{obs}},\alpha,\delta) &= \Phi_{\mathrm{ENA},1}(v_{\mathrm{obs}},\alpha,\delta) + \Phi_{\mathrm{ENA},2}(v_{\mathrm{obs}},\alpha,\delta)\\ &\simeq \Phi_{\mathrm{ENA},2}(v_{\mathrm{obs}},\alpha,\delta)\int_{r_1=r_s}^{r_2=r_H}\mathrm{d}r\, j_2(E_{\mathrm{ena}})\sigma_{\mathrm{ex}}(E_{\mathrm{ena}})n_{\mathrm{H}}.\end{aligned} \tag{31}$$

Here, v_{obs} is different from v due to the different reference frames, and the subscripts s and H denote the positions of the termination shock and the heliopause.

3.2. The inner heliosheath

After passing through the termination shock, the shocked solar wind is characterized by an effective Mach number smaller than 1, so that this downstream flow now can adapt to an outer pressure and can establish pressure equilibrium with the interstellar plasma at the heliopause. This, however, means that, in general, neither the direction nor the magnitude of the downstream plasma flow will be constant, introducing a complication for the line of sight integral in Eq. (31). Here we do not want to extract the resulting flow properties from numercial simulations, but want to take advantage of analytical representations offering satisfactory approximations for our purpose. For subsonic heliosheath flows with sufficiently low Mach numbers (i.e. $M_s \ll 1$), one can assume incompressibility of the plasma, and, besides some cooling due to charge exchange reactions, allowing us to derive the flow vector from a flow potential Φ. The simplest approach to this potential had first been introduced by Parker (1963), while a more general form discussed by Fahr & Fichtner (1991) accounts for much more general boundary conditions, while still delivering analytical representations of the plasma flow downstream of the shock.

In this more general case, the transformation between the reference frames given by Eq. (4) takes a more complicated form in the inner heliosheath, namely

$$v_{\mathrm{obs}} = v_{\mathrm{ena},2} - U_2\cos\beta(r,\alpha,\delta) = v_{\mathrm{ena},2} - U_{2,r}(r,\alpha,\delta), \tag{32}$$

with $\beta = \angle(\boldsymbol{U}(r,\alpha,\delta),\boldsymbol{e}_r(\alpha,\delta))$, i.e. the tilt angle of the local bulk velocity flow vector with respect to the local radian vector. Therefore, the ENA velocity required to specifically obtain v_{obs}-ENAs at the observer is no longer a constant expression, but a continuous function of the solar distance r and the heliospheric direction $\{\alpha,\delta\}$, ranging between the upstream velocity given by Eq. (4) for $\beta \simeq 0°$, down to $v_{\mathrm{obs}} = v_{\mathrm{ena},2}$ for $\beta \simeq 90°$. This latter configuration is commonly found near the heliopause (see also Fig. 1). The general formulation of the integrated ENA flux in this region follows from Eq. (29),

$$\Phi_{\mathrm{ENA},2}(v_{\mathrm{obs}},\alpha,\delta) = \frac{\sigma_{\mathrm{ex}}n_{\mathrm{H}}}{m}\int_{r_s}^{r_H}\mathrm{d}r\, j_2(v_{\mathrm{ena},2}(r,\alpha,\delta)), \tag{33}$$

where we have assumed that the charge exchange cross section and the neutral hydrogen density are approximately constant. Using Eqs. (30) and (21), this equation transforms into

$$\begin{aligned}\Phi_{\mathrm{ENA},2}(v_{\mathrm{obs}},\alpha,\delta) =& \frac{\sigma_{\mathrm{ex}}n_{\mathrm{H}}sU_1^5}{mC^{3/2}}f_{\mathrm{pui},0,1}(r_s,\alpha,\delta)\\ &\times\int_{r_s}^{r_H}\mathrm{d}r v_{\mathrm{ena},2}(v_{\mathrm{obs}},r,\alpha,\delta)^{-3}.\end{aligned} \tag{34}$$

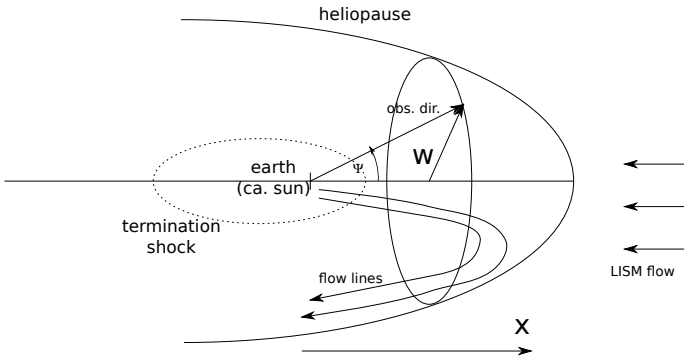

Fig. 1. The coordinate system used in the potential flow model for the plasma stream lines (not to scale).

Using Eq. (28), this expression transforms into

$$\Phi_{\mathrm{ENA},2}(v_{\mathrm{obs}},\alpha,\delta) = \frac{\xi_{\mathrm{s}}(0,0)\sigma_{\mathrm{ex}} n_{\mathrm{p,E}} n_{\mathrm{H}} s U_1^2}{2\pi m C^{3/2}} \left(\frac{r_{\mathrm{E}}}{r_{\mathrm{s}}(\alpha,\delta)}\right)^2 \times \int_{r_{\mathrm{s}}}^{r_{\mathrm{H}}} \mathrm{d}r v_{\mathrm{ena},2}(v_{\mathrm{obs}},r,\alpha,\delta)^{-3}. \quad (35)$$

Along any individual flow line, $f_{\mathrm{pui},0,2}$ should be constant due to the incompressibility of the downstream medium, and only along a line-of-sight crossing multiple non-radial flow lines is a modification due to frame-of-reference effects expected. Inserting Eq. (32), we thus obtain

$$\Phi_{\mathrm{ENA},2}(v_{\mathrm{obs}},\alpha,\delta) = \frac{\xi_{\mathrm{s}}(0,0)\sigma_{\mathrm{ex}} n_{\mathrm{p,E}} n_{\mathrm{H}} s U_1^2}{2\pi m C^{3/2}} \left(\frac{r_{\mathrm{E}}}{r_{\mathrm{s}}(\alpha,\delta)}\right)^2 \times \int_{r_{\mathrm{s}}}^{r_{\mathrm{H}}} \mathrm{d}r (v_{\mathrm{obs}} + U_r(r,\alpha,\delta))^{-3}. \quad (36)$$

3.3. The subsonic plasma flow in the inner heliosheath

To evaluate this expression, we require a profile for the individual plasma flow lines on the downstream side, i.e. an expression for $U_{2,r}(r,\alpha,\delta)$. In this study, we adopt the model by Fahr & Fichtner (1991), who described the inner heliosheath flow using a velocity potential field given by

$$\Phi_U(\boldsymbol{r}) = -\Gamma\left[\bar{z} - \frac{A + B\cos\Psi}{\sqrt{\bar{x}^2+\bar{w}^2}}\right] L, \quad (37)$$

where $L \simeq 150$ AU is the heliopause stand-off distance (i.e. the distance between the sun and the heliopause in the nose direction), the normalised axisymmetrical coordinates are denoted by $\bar{w} = w/L$ (for the distance perpendicular to the symmetry axis) and $\bar{x} = x/L$ (for the distance along the symmetry axis), and the angle Ψ of the line-of-sight with respect to the symmetry axis is defined by $\tan\Psi = \frac{\bar{w}}{\bar{x}}$. (For a graphical representation and definition of the coordinate system, see Fig. 1.) The factor Γ must be selected in a way that, at the TS, the velocity is exactly the solar wind velocity downstream of the shock, as this is the initial velocity with which the plasma is injected into the downstream region. It should be noted that the orientation of the z-coordinate axes is opposite to Fahr & Fichtner (1991), but due to the symmetry properties of the sin and tan functions, the resulting Ψ and r_{H} are always positive.

With free choices for the open flow parameters A and B, one can determine the net momentum outflow carried by the distant solar wind through a closed surface around the sun and thus the net force acting back on the solar system. For the special choice $2B = A$, no net force is operating, thus describing the situation that the solar system moves undecelerated through the interstellar medium, i.e. a state of motion that asymptotically in fact is approached by moving stellar-wind systems (see Fahr & Scherer 1995). Under these conditions, the subsonic flow lines in a large region of the heliosheath are quasi-radial and – besides a narrow region close to the heliopause – streamlines essentially do not cross the radial line-of-sight. This enables mathematical simplifications and is justified as long as the solar system moves through a homogeneous interstellar gas. Using spherical coordinates instead of cylindrical ones (where $\bar{r} = \sqrt{\bar{x}^2+\bar{w}^2}$), we obtain

$$\Phi_U(\boldsymbol{r}) = -\Gamma\left[\bar{r}\cos\Psi - \frac{A + B\cos\Psi}{\bar{r}}\right] L. \quad (38)$$

This expression allows us to find the radial velocity vector component

$$U_{2,r}(\alpha,\delta) = U_2\cos\beta(r,\alpha,\delta) = -\frac{\mathrm{d}}{\mathrm{d}r}\Phi_U(\boldsymbol{r}) = \Gamma\left[\cos\Psi + \frac{A + B\cos\Psi}{\bar{r}^2}\right]. \quad (39)$$

This relation now allows to write the normalization parameter Γ in an analytical form:

$$\Gamma = \frac{U_1(\alpha,\delta)}{s(\alpha,\delta)}\left[\cos\Psi_{\mathrm{s}}(\alpha,\delta) + \frac{A + B\cos\Psi_{\mathrm{s}}(\alpha,\delta)}{\bar{r}_{\mathrm{s}}^2(\alpha,\delta)}\right]^{-1} = \frac{U_1(\alpha,\delta)}{s(\alpha,\delta)}\tilde{\Gamma}(\alpha,\delta). \quad (40)$$

Applying a magnetohydrodynamic flow model would result in more realistic, but likewise more complex flow patterns; at this point, we have decided to adopt a hydrodynamic model mainly because it results in analytic expressions which can be evaluated more quickly and serve as a "first order approximation", which can be refined in future studies.

3.4. The line-of-sight integral in the inner heliosheath

Using this result and Eq. (32) then allows transform of Eq. (36) to

$$\Phi_{\mathrm{ENA},2}(v_{\mathrm{obs}},\alpha,\delta) = \frac{\xi_{\mathrm{s}}(0,0)\sigma_{\mathrm{ex}} n_{\mathrm{p,E}} n_{\mathrm{H}} s U_1^2 C^{-3/2}}{2\pi m}\left(\frac{r_{\mathrm{E}}}{r_{\mathrm{s}}(\alpha,\delta)}\right)^2 \times \int_{r_{\mathrm{s}}}^{r_{\mathrm{H}}} \mathrm{d}r\left(v_{\mathrm{obs}} + \Gamma\left(\cos\Psi + \frac{A + B\cos\Psi}{\bar{r}^2}\right)\right)^{-3}. \quad (41)$$

To evaluate this integral, we transform it in to the mathematically more compact form

$$\Phi_{\mathrm{ENA},2}(v_{\mathrm{obs}},\alpha,\delta) = \frac{\xi_{\mathrm{s}}(0,0)\sigma_{\mathrm{ex}} n_{\mathrm{p,E}} n_{\mathrm{H}} s U_1^2}{2\pi m C^{3/2}}\left(\frac{r_{\mathrm{E}}}{r_{\mathrm{s}}(\alpha,\delta)}\right)^2 \times \int_{\bar{r}_{\mathrm{s}}}^{\bar{r}_{\mathrm{H}}} \mathrm{d}r\left(a + \frac{b}{\bar{r}^2}\right)^{-3} = \frac{\xi_{\mathrm{s}}(0,0)\sigma_{\mathrm{ex}} n_{\mathrm{p,E}} n_{\mathrm{H}} s U_1^2}{2\pi m C^{3/2}}\left(\frac{r_{\mathrm{E}}}{r_{\mathrm{s}}(\alpha,\delta)}\right)^2 I(\alpha,\delta), \quad (42)$$

where we have introduced the $\{\alpha,\delta\}$-dependent factors

$$a = v_{\mathrm{obs}} + \Gamma\cos\Psi(\alpha,\delta) \simeq o(U_1) \quad (43)$$

and

$$b = \Gamma(A + B\cos\Psi(\alpha,\delta)) \simeq o(U_1), \tag{44}$$

and $\bar{r} = o(1)$. The order-of-magnitude estimates are correct for 1 keV ENAs in the observers rest frame. An analytical solution for this integral does exist in the form

$$\begin{aligned} I &= \left[\bar{r}\frac{8a^2\bar{r}^5 + 25ab\bar{r}^3 + 15b^2}{8a^3(a\bar{r}^2+b)^2} - \frac{15\sqrt{b}}{8a^{7/2}}\arctan\left(\sqrt{\frac{a}{b}}\bar{r}\right)\right]_{\bar{r}_\mathrm{s}}^{\bar{r}_\mathrm{H}} \\ &= \left[\bar{r}\frac{(3a\bar{r}^2+4b)^2 - (a\bar{r}^2-b)^2 - ab\bar{r}^2}{8a^3(a\bar{r}^2+b)^2}\right]_{\bar{r}_\mathrm{s}}^{\bar{r}_\mathrm{H}} \\ &\quad - \frac{15\sqrt{\frac{b}{a}}}{8a^3}\arctan\left(\sqrt{\frac{a}{b}}\frac{\bar{r}_\mathrm{H}-\bar{r}_\mathrm{s}}{1+\frac{a}{b}\bar{r}_\mathrm{s}\bar{r}_\mathrm{H}}\right). \end{aligned} \tag{45}$$

Obviously, to prevent complex-valued results due to negative roots from appearing, we need $ab > 0$. For the energy range of interest, it can be shown that this integral can be approximated by

$$I \simeq c(\bar{r}_\mathrm{H} - \bar{r}_\mathrm{s}) + d. \tag{46}$$

This analytical integral, which is a strongly nonlinear function due to $\Psi = \arctan(\bar{w}/\bar{x})$, can only be evaluated numerically. To determine the parameters already introduced, we need more model input to describe the geometry of the TS and the heliopause (HP), and also the compression ratio s and the magnetic field tilt angle θ at the termination shock. We introduce the models adopted for this in the following sections.

3.4.1. The Parker field and the magnetic field tilt angle

The standard model for the solar wind magnetic field goes back to Parker (1958), who derived a description of the solar magnetic field convected outwards with the solar wind, taking into account the angular momentum of the sun and the frozen-in field condition of MHD. Adopting spherical coordinates and the same orientation as introduced earlier for the angle Ψ (i.e. where the x-axis is oriented towards the heliospheric nose), and fixing the z-axis with the rotational axis of the sun, we obtain the parameterisation

$$\boldsymbol{B}_P \simeq \frac{B_0}{r}\left(\frac{1}{r}\begin{pmatrix}\cos\phi\cos\vartheta\\ \sin\phi\cos\vartheta\\ \sin\vartheta\end{pmatrix} + k\begin{pmatrix}-\sin\phi\cos\vartheta\\ \cos\phi\cos\vartheta\\ 0\end{pmatrix}\right), \tag{47}$$

where the angle ϑ is the heliospheric latitude, which is not precisely the same as the angle Ψ introduced earlier; Ψ is the angle between the LISM inflow direction (i.e. the x-axis) and the vector called $\boldsymbol{w}$ (see Fig. 1), while θ is the angle between the x-axis and the projection of $\boldsymbol{w}$ in the xz-plane. The parameter k is defined by

$$k = \frac{\Omega(\vartheta)}{U(\vartheta)}, \tag{48}$$

where Ω is the suns rotation frequency, $U(\vartheta)$ the (radial) solar wind flow velocity (which has observationally been found to be a function of the latitude ϑ during solar minimum conditions, see e.g. McComas et al. 2000), and r is the heliocentric distance, see Scherer & Fahr 2009). A typical value for this parameter applicable to solar wind conditions near the TS is $k = 1.08025\ \mathrm{AU}^{-1}$. At distances of the order of 90 AU (i.e. the distance to the TS in the nose direction of the heliosphere), the first term may be safely ignored, and the magnetic field is mostly azimuthal. To evaluate the magnetic field tilt angle $\theta = \angle(\boldsymbol{B}, \boldsymbol{n})$, we also need to know the normal to the heliospheric shock surface. Unfortunately, due to a lack of observational data, we are restricted to (magneto-)hydrodynamic models which are based on varying degree of physical sophistications. One of the most recent models for the geometry of the TS has been derived by Borrmann & Fichtner (2005); in this study, we make use of the analytic approximation of the aforementioned model by Fahr et al. (2008), who describe the TS as a best-fitting ellipsoid with two identical short (104.7 AU) and one long (133.5 AU) semi-major axes. This model also allows to derive the TS distance, $\bar{r}_\mathrm{s}$.

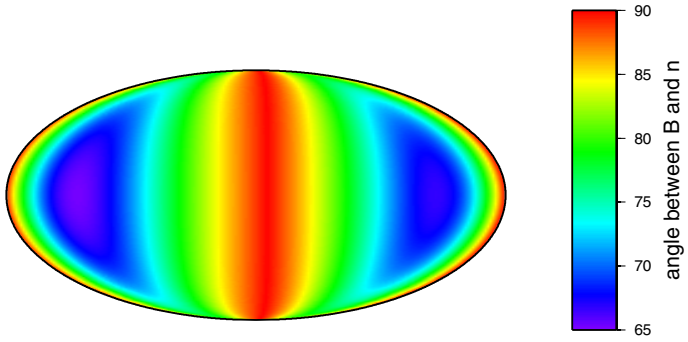

Fig. 2. The magnetic field tilt angles.

More realistic models for the solar wind magnetic field will be applied in future studies. One comparatively easy model, which can still be performed without complex numerical simulations would be the magnetic field model derived by Fisk (1996), which takes into account a more realistic dynamics of the magnetized surface of the sun.

Combining these two models, we are able to derive the magnetic field tilt angle numerically (see in Fig. 2); as a basic result, the magnetic field tilt angle $\theta_{Bn}(\alpha,\delta)$ varies between 65° in the rear flanks and 90° in the nose and tail regions.

3.4.2. The compression ratio

Another relevant parameter appearing in this study is the MHD compression ratio, $s = \rho_2/\rho_1$. Deriving this parameter would in principle require setting up and solving the MHD jump conditions, with a special emphasis on the PUI component (i.e. a multifluid approach to the jump conditions). However, for the special configuration studied here, Fahr & Chalov (2008) found that, within a hydrodynamic two-fluid approach, the compression ratio is given by Eq. (5) ($s \simeq 2.6\sqrt{M_{\mathrm{pui},1}}$), i.e. is a function of the upstream pick-up ion sonic Mach number.

On the other hand, the solar wind termination shock is a *magneto*hydrodynamic shock, i.e. the Alfvenic Mach number must be taken into account as well, complicating the physics of the shock transition especially in the case of quasiparallel shocks. The two relevant Mach numbers appearing in the full MHD description are defined by

$$M_\mathrm{s} = \frac{U}{v_\mathrm{s}} \tag{49}$$

for the sonic Mach number, where v_s is the velocity of sound, and the Alfvenic Mach number

$$M_\mathrm{A} = \frac{U}{v_\mathrm{A}}, \tag{50}$$

based on the Alfven velocity v_A. As already pointed out earlier, the upstream PUIs are marginally subsonic (see Fahr & Chalov 2008; Lee et al. 2009), i.e. $M_{s,\mathrm{pui},1} \simeq 1$, and any significant deviation from the hydrodynamic model in more parallel shock conditions must therefore be a result of the Alfvenic Mach number; an "effective" Mach number may be defined using

$$M_{\mathrm{eff}} = \sqrt{M_s^2 + M_A^2} \simeq \max(1, M_A). \tag{51}$$

Unfortunately, no globally valid relation between the Mach numbers and the compression ratio exists, especially in a multifluid (potentially temperature-anisotropic) MHD system. Therefore, we restrict ourselves to the hydrodynamic approach (Eq. (5)), using the effective speed of sound ($v_s \stackrel{\mathrm{def}}{=} \partial p/\partial\rho$), which in our system is given by

$$v_{s,\mathrm{eff}} \simeq \sqrt{\frac{\partial p_{\mathrm{pui}}}{\partial \rho_{\mathrm{sw}}}}. \tag{52}$$

The pickup ion pressure follows from Eqs. (13) and (28),

$$p_{\mathrm{pui}} = \xi_s(0,0)\rho_{\mathrm{sw}}(r)U_1^2 \ln\left(\frac{v_\infty}{U_1}\right). \tag{53}$$

Therefore, the effective velocity of sound is given by

$$v_{s,\mathrm{eff}} = U_1 \sqrt{\xi_s(0,0)\ln\left(\frac{v_\infty}{U_1}\right)}, \tag{54}$$

and the Mach number is given by

$$M_s = \sqrt{\xi_s(0,0)\ln\frac{v_\infty}{U_1}^{-1}}, \tag{55}$$

while the hydrodynamic compression ratio transforms into

$$s \simeq 2.6\left(\xi_s(0,0)\ln\left(\frac{v_\infty}{U_1}\right)\right)^{-1/4}. \tag{56}$$

Therefore, the compression ratio of the pickup ions only depends on the PUI abundance (which is approximately constant) and the solar wind speed. For a sufficiently high upper cutoff velocity $v_\infty \gg U_1$, the logarithm can also be approximated as constant within typical solar wind variations over a solar cycle (and including the latitude-dependent solar wind speed).

The multifluid model used here has been developed, over a decade (see e.g. Chalov & Fahr 1994, 1995, 1997; Fahr et al. 2000; Fahr & Chalov 2008), using increasingly more appropriate and sophisticated multi-fluid shock modelling including SW protons and electrons, PUIs and ACRs as separate fluids. In this model, different types of ions are described by separate fluids, which are coupled dynamically and thermodynamically by adequate conservation relations. This consistent multi-fluid approach allows us to derive, with great accuracy, the behaviour of PUIs passing the TS in the presence of a thermal core of solar wind ions. We do not expect any significant variations due to microphysics kinetics of the multicomponent shock.

3.4.3. The position of the heliopause

The precise structure of the outer heliosphere, i.e. beyond the TS, is even less understood than the geometry of the termination shock, since the most distant missions to probe this region, i.e. the Voyagers, have not yet reached the heliopause. However, it is possible to estimate the position of the heliopause based on existing inner heliosheath models, such as the model developed by Fahr et al. (1988), which has already been used earlier to describe the radial component of the plasma flow velocity. Using this model, the location of the heliopause here can be calculated as

$$r_H \simeq \frac{\Psi}{\sin\Psi} L, \tag{57}$$

or

$$\bar{r}_H \simeq \frac{\Psi}{\sin\Psi}, \tag{58}$$

for $A = 2B$, i.e. a solar system moving at constant velocity through the interstellar medium, without any acceleration or deceleration.

This model describes an open heliotail, where the outer distances in the tail approach infinity, which might result in unphysical results since the energetic ENAs only have a finite lifetime before reionisation, which is not taken into account in this study. On the other hand, the TS in this region is significantly more distant than in the nose region, and the PUI density will be accordingly smaller there as well (due to dropping off according to r^{-2}). Due to these effects, the ENA fluxes in the tail region are expected to be significantly smaller, and we continue using this model even in the heliotail, cutting off the line-of-sight integral at approximately the ENA extinction length, which we estimate to be 300 AU, i.e. twice the nose distance to the HP.

We also need to point out that our representation of the heliospheric boundary layers (i.e. the TS and the HP geometry) are based on hydrodynamic models. An improved, magnetohdyrodynamic description, including more realistic representations due to tilted LISM fields, may certainly change the outcome, including (but not limited to) breaking the axisymmetry assumed in the present study. This may increase the overall match with IBEX data, and will be investigated in a future study.

Another interesting point is that the latest findings by Voyager (Krimigis et al. 2011) seem to suggest that the heliopause might be closer to us than expected from earlier theoretical modelings (130 AU, in contrast to the 150 AU used here). However, it is also possible that the heliopause is not a narrow surface, but made of an extended pre- and post-HP region, as predicted theoretically by e.g. Fahr & Neutsch (1983). Until existing models have been modified for recent Voyager measurements, we will continue using a value of 150 AU.

3.5. ENA fluxes from the inner heliosheath

Before we evaluate the equations derived in the preceeding sections, we study the qualitative behaviour of the integrated ENA flux. Ignoring constant factors, Eq. (36) tells us that

$$\Phi \propto D(\alpha,\delta)I(\alpha,\delta) = sC^{-3/2}(\theta,s)\frac{U_1^2}{r_s^2}I(\alpha,\delta), \tag{59}$$

where we have introduced the new factor $D(\alpha,\delta)$ which encompasses all relevant contributions to the direction-dependent ENA flux that do not depend upon the line-of-sight integral.

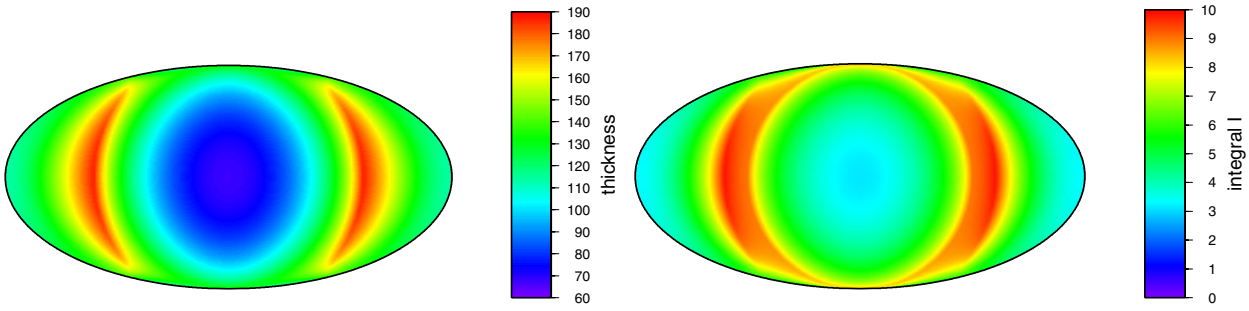

(a) The inner heliosheath thickness $r_H - r_s$. (b) $I(\alpha, \delta)$.

Fig. 3. The contributions to the ENA flux due to the integral $I(\alpha, \delta)$. The heliopause distance, which grows infinite in the tail region, has been cut off at 300 AU.

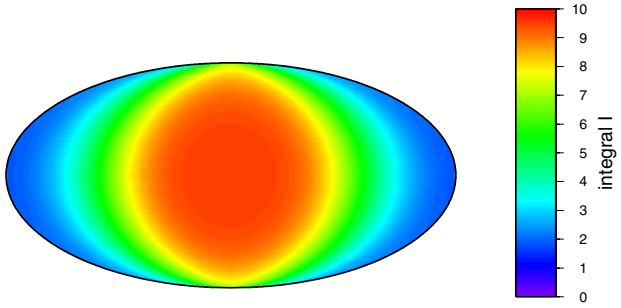

(a) $D(\alpha, \delta)$.

Fig. 4. The contributions to the ENA flux due to the factor $D(\alpha, \delta)$.

From the earlier study following Eq. (45), it is possible to estimate that, to first order, the integral behaves as $I \simeq c\Delta(\bar{r}_H - \bar{r}_s) + d$, i.e. this contribution is proportional to the thickness of the inner heliosheath measured along a line-of-sight. Therefore, this factor results in an ENA flux increasing according to $\Delta\bar{r} = \bar{r}_H - \bar{r}_s$, which should contribute significantly in the heliotail. This behaviour can be easily recognised in Fig. 3, where we present the inner heliosheath thickness, and the resulting line-of-sight integrals $I(\alpha, \delta)$. The second factor, $D(\alpha, \delta)$, is overcompensating this behaviour due to a drop according to $\bar{r}_s^{-2}$, which, again, is expected to appear dominantly in the heliotail, resulting in a total drop according to $\bar{r}_s^{-1}$. The behaviour of this factor is demonstrated in Fig. 4.

Finally, combining both factors (and also including the constant factors left out in the last paragraph), and adopting $\sigma_{ex} \simeq 2 \times 10^{-15}$ cm^2, $n_H \simeq 0.1$ cm^{-3} and $n_{p,E} \simeq 4$ cm^{-3} as standard values for the remaining parameters appearing in Eq. (42), we obtain the absolute ENA fluxes presented in Fig. 5, which clearly exhibit a pronounced ringlike emission region qualitatively similar to the IBEX observations, and also a strong dependence on the solar wind speed and its latitudinal variation. This behaviour can be easily understood by noting that, in the narrow ring-like region emerging near $\alpha = \pm 90°$, the contribution due to $I(\alpha, \delta)$ already starts to increase as the heliopause starts to be pushed further outwards, while the TS position is still mostly constant, within 90–100 AU, and the contribution due to $D(\alpha, \delta)$ does not significantly contribute yet. Further in the tail, however, the quadratic drop of the TS distance takes over, and the ENA fluxes are diminished again.

The absolute values of these ENA fluxes also exhibit an interesting behaviour. First, we see that the ring-like radiation feature is more intense by a factor of about 2 compared to the background in the nose region, which, in good approximation, equals the ratio found between the IBEX ribbon and the IBEX nose region (McComas et al. 2009a), suggesting that the process discussed in this study may in fact be responsible for the observed phenomenon. The absolute intensities of the predicted ENA fluxes are also remarkably close to the observed absolute IBEX values. Averaging over local fluctuations, the IBEX ribbon at 1 keV has an ENA flux of about 200 cm^{-2} s^{-1} sr^{-1} keV^{-1}, while the average globally distributed flux is found at 100 cm^{-2} s^{-1} sr^{-1} keV^{-1}. Comparing these absolute values to those found in this study, i.e. 350 cm^{-2} s^{-1} sr^{-1} keV^{-1} on the ring and 200 cm^{-2} s^{-1} sr^{-1} keV^{-1} in the nose region, we see that our absolute numerical values are remarkably close to the observed data, within a factor of less than 2. In addition, assuming that a latitude-dependent solar wind speed allows interruptions in the ring-like structure (see Fig. 5c), we obtain an emission feature which is even closer to the IBEX ribbon.

The main difference between these model results and the IBEX observations that can not be identified in the framework of this first study is a misplacement of the emission feature on the sky. However, considering that the present model calculations are based on strongly idealised (i.e. axisymmetric) models of the form and position of the termination shock and the heliopause, which, as hinted by the Voyager missions, are considerably more dynamic than initially expected, the effective boundaries in the line-of-sight integral (Eq. (29)) surely deviate from those used in this basic model. In addition, the solar wind speed at high latitudes at the TS is not known; instead, this study uses an extrapolation of Ulysses data to greater distances, assuming that the solar wind speed remains constant until directly before the shock. More realistic models are required to refine the underlying ENA generation mechanism studied here.

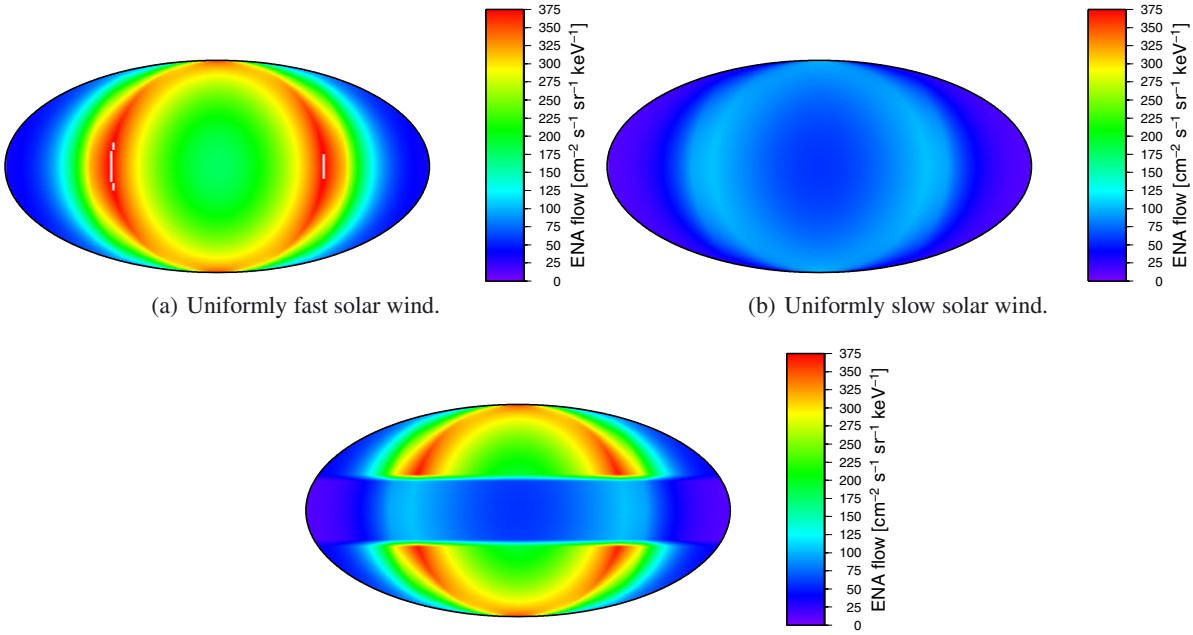

(a) Uniformly fast solar wind.

(b) Uniformly slow solar wind.

(c) Latitude-dependent solar wind as seen by e.g. Ulysses.

Fig. 5. The ENA fluxes produced by the mechanism studied here and different models for the solar wind speed.

4. Discussion

We have investigated the possibility that the IBEX ribbon feature is generated beyond the solar wind termination shock (TS) by shock-processed thermaly heated pick-up ions as the ENA source population. Interestingly, even though the precise placement of the feature does not match the position of the IBEX ribbon, the absolute values of the predicted fluxes, as well as the ratio between the active region and the background agree quite well with the absolute values detected by IBEX, within a factor of less than 2. Considering that the present study is based on several idealized assumptions of the heliospheric boundary layers, this difference may result from just these simplifications, and a more realistic heliospheric model might improve the match. The main differences between our model and existing approaches found in literature is a more careful treatment of the TS, which allows to derive explicit formulations for the MHD compression and the PUI pressures. This effect is strongly sensitive to the geometry of the outer heliosphere (i.e. the TS and also the heliopause), ultimately resulting in a ring-like structure which exhibits a strong resemblance to the IBEX ribbon feature, except for some symmetry-breaking deformations. This feature is a property of the heliospheric interface and does not depend on the spectral shape of the source plasma (except, of course, with respect for absolute ENA fluxes and the spectral shape of the ENA flows – which will be the focus of a future study).

One effect which definitely perturbs the geometry of the heliosphere is MHD stresses connected with the LISM B-field. This effect strongly perturbs the overall geometry of the heliopause, but much less the geometry of the termination shock. As seen in Izmodenov & Alexashov (2005, 2006), even strong LISM magnetic fields inclined by 45 degrees with respect to the LISM only marginally change the radial location of the TS, and has little effect on the symmetry of the TS surface (see also Izmodenov & Baranov 2006, pp. 67–135.)

In addition, the high sensitivity of the ENA fluxes to heliospheric parameters, i.e. the solar wind speed near the TS and the solar distance of the TS and the HP, may offer a unique possibility to trace remotely the fine structure of the heliospheric boundary layers. A full-sky fit of the individual parameters of the model presented here seems highly promising in the context of an improved ENA generation model, which should also take into account secondary reionisation processes in the heliotail and a more flexible approach for the solar wind speed near the TS.

Independent of details related to the solar wind magnetic field orientation and the TS position, one also has to take into account that the position of the TS is mostly determined by a balance of ram pressures, i.e. the solar wind speed, which will likewise leave an imprint on the shock physics; the recent results obtained by Voyager clearly demonstrate that fixing one unique position of the TS may be quite problematic (Stone et al. 2008). Another point which needs to be taken into careful account is the Alfven Mach number,

$$M_{\rm A} \propto U\frac{\sqrt{n}}{B}, \tag{50}$$

which directly influences the properties of the termination shock (i.e. the compression ratio s). Considering that, according to the standard model for the solar wind, the Parker field behaves as r^{-1} in the ecliptic plane, but as r^{-2} near the poles, a latitude-dependent variation of the compression ratio, and ultimately, of the resulting ENA fluxes must be expected. This effect is enhanced by the observational fact that, during solar minimum conditions, the solar wind speed U_1, upstream of the TS, is not constant, but also function of the heliospheric latitude θ (McComas et al. 2000).

It is also be important to remember that our calculations were restricted to the assumption of a strict axi-symmetry with respect to the upwind LISM flow axis. This symmetry is broken by the LISM magnetic fields tilted with respect to the LISM inflow direction (McComas et al. 2009a; Schwadron et al. 2009). Such fields exert MHD stress forces which enforce the usage of 3D-MHD modellings like those developed by Ratkiewicz et al. (2006); Pogorelov (2006); Izmodenov & Alexashov (2006); Opher et al. (2006). The influence of such MHD stresses is only

weakly pronounced on the shape of the termination shock for interstellar magnetic field strengths up to 2.5 μG (as found in 3D MHD simulations performed by Izmodenov & Alexashov 2006), which can not explain the TS asymmetries indicated by Voyager-1 and -2. Similar studies by Opher et al. (2009) found that, for stronger interstellar magnetic fields (between 3.7 and 5.5 μG), stress forces result in a deformation of the heliosphere, allowing to reproduce the termination shock positions encountered by Voyager-1 and -2. However, at the moment, there are no clear informations about the nature of these perceived asymmetries available, neither by theory nor observations. Voyager-1 and -2 only deliver two single event points, separated by about 2 years in time; whether the difference in TS positions found are due to time-variabilities in the solar wind ram pressures or in persistent TS asymmetries, thus is not clear. Nevertheless, whatever stress forces are acting on the TS, they at the very minimum influence the distance scale to the termination shock and the geometry of the heliopause. As we have shown, both these factors directly influence the ENA fluxes with sources in the heliosheath and thus might less influence the absolute flux intensities, than the location of the pronounced ENA features. Here one could easily expect a significant improvement of theoretical data fits with a combination of our present model calculations and those presented by Prested et al. (2010) which take into account MHD asymmetries, but model the sheath plasma with an ad hoc assumption of kappa-distributed pick-up ions.

Another symmetry break is in principle imprinted on the heliospheric boundary system due to the latitudinally variable solar wind properties. In our model above we have taking this variation into account, however keeping to an axisymmetric HD termination shock model. Scherer & Ferreira (2005) have taken into account an axisymmetric approximation of the solar wind latitude variation in their HD modelling; they were able to demonstrate that this induces a kink in the surface of the termination shock at medium latitudes, changing the magnetic tilt angles in these regions to which downstream pick up ion temperatures react very sensitively. However, before applying this model, it should be improved to an non-axisymmetric model of the latitude variation of the solar wind ram pressure in order to come closer to a true solar minimum configuration as it has been seen by IBEX in the past years.

In this paper we also have not yet studied extended energy spectra from 0.1 to 10 keV, covering the full energy range accessible by IBEX, but we focused on ENA fluxes around 1 keV instead (i.e. approximately where the available data has the best statistics). While the first IBEX results suggested that the spectral index is surprisingly smooth and approximately constant across the sky (i.e. the ribbon did not seem to stand up as a special feature in this parameter, see McComas et al. 2009a), more recent studies on the basis of three consecutive IBEX full sky maps, however, do suggest that a systematic difference between the spectral properties of the distributed fluxes of the background and those of the ribbon can be identified (see Schwadron et al. 2011; Livadiotis et al. 2011). Schwadron et al. (2011) addressed this as a "knee"-like spectral feature appearing both in the ribbon and the background between 1 and 6 keV with different spectral locations of the knee and different spectral power indices.

Another recent observational result (Schwadron et al. 2011) concerns ENA background fluxes showing a weaker spectrum and small spectral intensities towards the heliotail compared to the flanks and the nose of the heliosphere. This can be explained by our present model as due to the fall-off of upstream pick-up proton densities serving as the seed of energetic downstream protons, dropping in density with increasing radial solar distance to the shock. Finally, analysis of observed IBEX data shows some ordering with the ecliptic latitude and suggests some connection to solar wind structures (McComas et al. 2009a; Schwadron et al. 2011). Thus galactic sources for these ENAs according to this finding seem to be only of a more latent nature, while a production process much closer in, correlated with the heliosheath plasma population seems much more likely. This is consistent with the assumption of this model presented here.

In an upcoming study, we will derive full ENA flow spectra following from both PUI-related contributions, i.e. the shock-processed contribution studied here and the contribution due to cooled ACRs (Fahr et al. 2011), carefully examining the possibility that the IBEX data – especially the knee observed in the ribbon spectra – is a result of multiple processes which are superimposed.

Our model suggests that we will be able to see the transition from the current minimum of the solar-cycle towards the upcoming maximum, expected to be reached in 2013 (i.e. it should be reflected in data in 2014–2015), offering a new and unique possibility for remote tracing of the heliospheric interface. This offers a way to test the reliability of this model over the next few years. Since the solar wind speed – especially its latitude dependence – is modulated by the solar cycle, the coming solar maximum in the following years should be reflected in the IBEX ENA skymaps, and also in INCA-Cassini data (Krimigis et al. 2009). Since the ENA fluxes derived in this model strongly depend on the positions of the TS and the HP, which in turn are – among other parameters – a function of the solar wind ram pressure, it can be expected that these positions will be modified when entering the solar maximum. This idea was also used as an explanation for the different distances at which the Voyagers encountered the TS (Jokipii 2008). Based on the mechanism studied here, the IBEX ribbon feature should transform in a more intense, more homogeneous circle (or ellipse), with an increased ENA flux detected in all energy ranges. Should this correlation not emerge, the heliosheath as source of IBEX keV ENAs are becoming more unlikely, which will place constraints on a set of properties of the outer heliosphere and the local interstellar medium, such as the hydrogen density and the pickup ion distribution.

Interesingly, Prested et al. (2010), while using comparable assumptions, did not see a narrow ENA feature such as that derived in this study. One significant difference to the present study is the absence of the frame-of-reference effect (Eq. (4)), which provides a significant imprint to the ENA fluxes. In addition, the ring-like feature obtained in this study is strongly correlated to the geometric shape of the TS and the HP; depending on the specific approaches to these geometries, the features may be different.

Acknowledgements. One of the authors, M. Siewert, is grateful to the Deutsche Forschungsgemeinschaft for financial support granted to him in the frame of the project Si-1550/2-1. D. J. McComas and N. A. Schwadron were supported by NASAs Explorers Program as a part of the IBEX mission. This research benefited greatly from discussions that were held at the meetings of the International Team devoted to understanding the v^{-5}-tails and ACRs that has been sponsored by the International Space Sciences Institute (ISSI) in Bern, Switzerland.

References

Borrmann, T., & Fichtner, H. 2005, Adv. Space Res., 35, 2091
Chalov, S. V., & Fahr, H.-J. 1994, A&A, 288, 973
Chalov, S. V., & Fahr, H.-J. 1995, Planet. Space Sci., 43, 1035
Chalov, S. V., & Fahr, H.-J. 1997, A&A, 326, 860
Chalov, S. V., & Fahr, H. J. 2011, Adv. Space Res., 47, 1523
Chalov, S. V., Alexashov, D. B., McComas, D., et al. 2010, ApJ, 716, L99

Dayeh, M. A., Desai, M. I., Dwyer, J. R., et al. 2009, ApJ, 693, 1588
Decker, R. B., Krimigis, S. M., Roelof, E. C., et al. 2005, Science, 309, 2020
Decker, R. B., Krimigus, S. M., Roelof, E. C., et al. 2008, Nature, 454, 67
Erkaev, N. V., Vogl, D. F., & Biernat, H. K. 2000, J. Plasma Physics, 64, 561
Fahr, H.-J. 2007, Ann. Geophys., 25, 2649
Fahr, H.-J., & Chalov, S. V. 2008, A&A, 490, L35
Fahr, H., & Scherer, K. 2004, AS&S, 1, 3
Fahr, H.-J., & Fichtner, H. 1991, Space Sci. Rev., 58, 193
Fahr, H. J., & Neutsch, W. 1983, MNRAS, 205, 839
Fahr, H. J., & Ruciński, D. 1999, A&A, 350, 1071
Fahr, H. J., & Scherer, K. 1995, Ap&SS, 225, 21
Fahr, H.-J., & Siewert, M. 2010a, ASTRA, 7, 1
Fahr, H.-J., & Siewert, M. 2010b, A&A, 512, A64
Fahr, H. J., Grzedzielski, S., & Ratkiewicz, R. 1988, Ann. Geophys., 6, 337
Fahr, H. J., Kausch, T., & Scherer, H. 2000, A&A, 357, 268
Fahr, H. J., Scherer, K., Potgieter, M. S., & Ferreira, S. E. S. 2008, A&A, 486, L1
Fahr, H., Chashei, I. V., & Verscharen, D. 2009, A&A, 505, 329
Fahr, H.-J., Siewert, M., McComas, D. J., & Schwadron, N. A. 2011, A&A, 531, A77
Fisk, L. A. 1996, J. Geophys. Res., 101, 15547
Fisk, L. A., & Gloeckler, G. 2008, ApJ, 686, 1466
Funsten, H. O., Allegrini, F., Crew, G. B., et al. 2009, Science, 326, 964
Fuselier, S. A., Allegrini, F., Funsten, H. O., et al. 2009, Science, 326, 962
Gloeckler, G. 2003, in Solar Wind Ten, ed. M. Velli, R. Bruno, F. Malara, & B. Bucci, AIP Conf. Ser., 679, 583
Gruntman, M., Roelof, E. C., Mitchell, D. G., et al. 2001, J. Geophys. Res., 106, 15767
Grzedzielski, S., Bzowski, M., Czechowski, A., et al. 2010, ApJ, 715, L84
Heerikhuisen, J., Pogorelov, N. V., Florinski, V., Zank, G. P., & le Roux, J. A. 2008, ApJ, 682, 679
Heerikhuisen, J., Pogorelov, N. V., Zank, G. P., et al. 2010, ApJ, 708, L126
Izmodenov, V. V., & Alexashov, D. 2005, in Solar Wind 11/SOHO 16, Connecting Sun and Heliosphere, ed. B. Fleck, T. H. Zurbuchen, & H. Lacoste, ESA SP, 592, 351
Izmodenov, V. V., & Alexashov, D. B. 2006, in Physics of the Inner Heliosheath, ed. J. Heerikhuisen, V. Florinski, G. P. Zank, & N. V. Pogorelov, AIP Conf. Ser., 858, 14
Izmodenov, V. V., & Baranov, V. B. 2006, ISSI Scientific Reports Series, 5, 67
Izmodenov, V. V., Malama, Y. G., Ruderman, M. S., et al. 2009, Space Sci. Rev., 146, 329
Jokipii, J. R. 2008, Nature, 454, 38
Krimigis, S. M., Mitchell, D. G., Roelof, E. C., Hsieh, K., & McComas, D. J. 2009, AGU Fall Meeting Abstracts, SH31B
Krimigis, S. M., Roelof, E. C., Decker, R. B., & Hill, M. E. 2011, Nature, 474, 359
Lee, M. A., Fahr, H. J., Kucharek, H., et al. 2009, Space Sci. Rev., 146, 275
Livadiotis, G., McComas, D. J., Dayeh, M. A., Funsten, H. O., & Schwadron, N. A. 2011, ApJ, 734, 1
McComas, D. J., & Schwadron, N. A. 2006, Geophys. Res. Lett., 33, 4102
McComas, D. J., Barraclough, B. L., Funsten, H. O., et al. 2000, J. Geophys. Res., 105, 10419
McComas, D., Allegrini, F., Bochsler, P., et al. 2004, in Physics of the Outer Heliosphere, ed. V. Florinski, N. V. Pogorelov, & G. P. Zank, AIP Conf. Ser., 719, 162
McComas, D. J., Allegrini, F., Bartolone, L., et al. 2006, in Physics of the Inner Heliosheath, ed. J. Heerikhuisen, V. Florinski, G. P. Zank, & N. V. Pogorelov, AIP Conf. Ser., 858, 241
McComas, D. J., Allegrini, F., Bochsler, P., et al. 2009a, Science, 326, 959
McComas, D. J., Allegrini, F., Bochsler, P., et al. 2009b, Space Sci. Rev., 146, 11
McComas, D. J., Elliott, H. A., & Schwadron, N. A. 2010, J. Geophys. Res. (Space Physics), 115, 3102
Opher, M., Stone, E. C., Liewer, P. C., & Gombosi, T. 2006, in Physics of the Inner Heliosheath, ed. J. Heerikhuisen, V. Florinski, G. P. Zank, & N. V. Pogorelov, AIP Conf. Ser., 858, 45
Opher, M., Bibi, F. A., Toth, G., et al. 2009, Nature, 462, 1036
Parker, E. N. 1958, ApJ, 128, 664
Parker, E. N. 1963, Interplanetary dynamical processes (New York: Interscience Publishers)
Pogorelov, N. V. 2006, in Physics of the Inner Heliosheath, ed. J. Heerikhuisen, V. Florinski, G. P. Zank, & N. V. Pogorelov, AIP Conf. Ser., 858, 3
Prested, C., Schwadron, N., Passuite, J., et al. 2008, J. Geophys. Res. (Space Physics), 113, A06102
Prested, C., Opher, M., & Schwadron, N. 2010, ApJ, 716, 550
Ratkiewicz, R., Grygorczuk, J., & Ben-Jaffel, L. 2006, in Physics of the Inner Heliosheath, ed. J. Heerikhuisen, V. Florinski, G. P. Zank, & N. V. Pogorelov, AIP Conf. Ser., 858, 27
Reisenfeld, D. B., Abell, T. R., Allegrini, F., et al. 2009, AGU Fall Meeting Abstracts, SH31B
Richardson, J. D., Kasper, J. C., Wang, C., Belcher, J. W., & Lazarus, A. J. 2008, Nature, 454, 63
Scherer, K., & Fahr, H. 2009, A&A, 495, 631
Scherer, K., & Fahr, H. J. 2003, Geophys. Res. Lett., 30, 020000
Scherer, K., & Ferreira, S. E. S. 2005, AS&S Trans., 1, 17
Schwadron, N. A., Bzowski, M., Crew, G. B., et al. 2009, Science, 326, 966
Schwadron, N. A., Allegrini, F., Bzowski, M., et al. 2011, ApJ, 731, 56
Siewert, M., & Fahr, H.-J. 2008, A&A, 485, 327
Sternal, O., Fichtner, H., & Scherer, K. 2008, A&A, 477, 365
Stone, E. C., Cummings, A. C., McDonald, F. B., et al. 2008, Nature, 454, 71
Vogl, D. F., Langmayr, D., Erkaev, N. V., et al. 2003, Planet. Space Sci., 51, 715